Deep Moist Convection at Upper Tropospheric Moisture Gradients - a Possible Involvement of Moist Symmetric Instabilities

Thomas Krennert [1], Alexander Jann [2], Central Institute for Meteorology and Geodynamics, Vienna, Austria

Introduction: An overall conditionally unstable stratification during a period of weak low level pressure gradient (fair weather) may be favourable to the onset of convective overturning above ground. An air parcel situated at higher elevations (mountains, hills) needs less energy and heating in order to become buoyant and starting to rise. Later, the onset of convective overturning will begin also in flat regions. If there is enough lift, an air parcel may reach saturation earlier or later, given the initial level of topographical height (See **Fig.1**, central and eastern Europe). Two ingredients, in combination with given instability, are necessary for the air parcel in order to reach ist Level of Free Convection (LFC): Sufficient moisture from ground levels, supplying the growing cell within regions of conditional instability, and / or sufficient lift in case of less sufficient moisture supply from the ground.

It can be assumed that the fair weather convection is faced with weaker favourable conditions regarding these two ingredients:

Overall moisture supply is less than e.g. during a prefrontal situation in summer season, when the formation of thunderstorms at the southern Alpine flank is most likely, because of increased moisture advection provided by a distinct southerly or a south-westerly stream at low- and mid-tropospheric levels.

Former investigations showed a strong vertical gradient of relative humidity between 600 and 400 hPa (derived from soundings, found in 90% of all cases). In upper regions a distinct horizontal gradient is depicted by the moisture gradients in the WV image. Therefore it may be concluded that entrainment becomes stronger at the vertical moisture gradient and also seems to vary at upper levels in the vicinity of the gradient between moist and dry regions in the WV image.

Fig.2 shows first signs of Deep Moist Convection (DMC) which is connected to a turbulent dark WV feature over Austria, the Czech Republic and Poland. The case of 9 July 2006 is representative for all ~75 investigated cases.

Fig. 1: (below), MSG HRVIS channel 12, 9 July 2006, at 0900 UTC, Austria indicated by red borderline; distinct frotal zone over western Europe; convective activity (mostly shallow convection, not reaching above 3000m) over the eastern Alpine region, Germany, Czech Republic, Poland, the Carpathian mountains and over Greece.

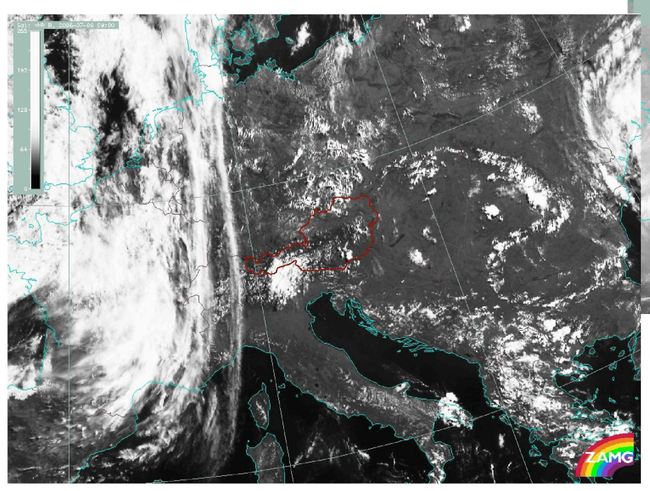

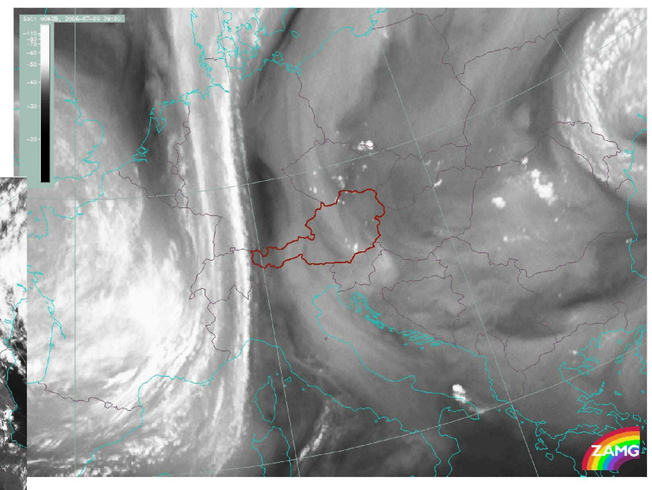

Fig. 2: (above), MSG Water Vapour channel 6.2µ, 9 July 2006, at 0900 UTC; few cells of deep moist convection (DMC, reaching above 5000m) over Austria and the Czech Republic can be seen. The cells clearly appear in connection to a darker zone in the WV image

Dry symmetric instability can be seen as a generalization of both inertial instability and dry (absolute) gravitational instability. Likewise, the Conditional Symmetric Instability (CSI) is a combination from inertial instability and conditional gravitational instability (criteria expressed in equations **E 1 - 4**), where M_g is the geostrophic absolute momentum of a geostrophically balanced mean state, v_g is the geostrophic wind in the direction perpendicular to the temperature gradient (the direction along an elongated baroclinic zone), f is the Coriolis parameter and x is the cross-front distance, increasing toward warmer air. Assuming that the geostrophic wind is constant in the direction along an elongated baroclinic zone, and inertial and conditional instabilities are absent, it can be shown that extending the M_g - Θ_e relationship (**E1-E4**) for CSI is equivalent to the negative saturated geostrophic potential vorticity criterion (Equations **E5, E6**), also known as the saturated equivalent geostrophic potential Vorticity EPV_g (e.g. Hoskins, 1974; Mc Cann, 1995).

E1) $$\left.\frac{d\Theta_{es}}{dz}\right|_{M_g} < 0$$

E2) $$\left.\frac{dM_g}{dx}\right|_{\Theta_{es}} < 0$$

E3) $$\Gamma_{moist}\big|_{M_g} < -\left.\frac{dT}{dz}\right|_{M_g} < \Gamma_{dry}\big|_{M_g}$$

E4) $$M_g = v_g + fx$$

E5) $$EPV_g < 0$$

E6) $$EPV_g = g\eta_g \cdot \nabla\Theta_{es}$$

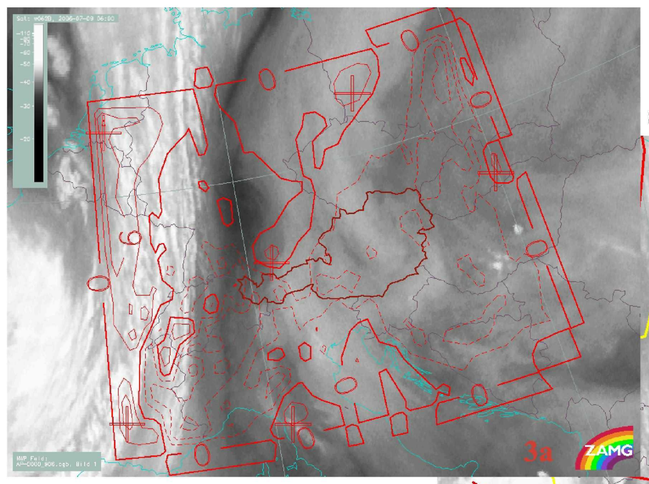

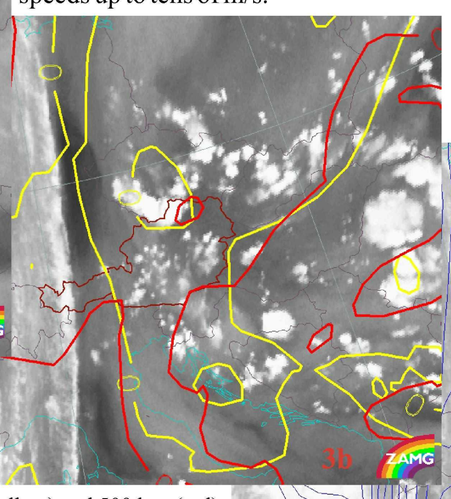

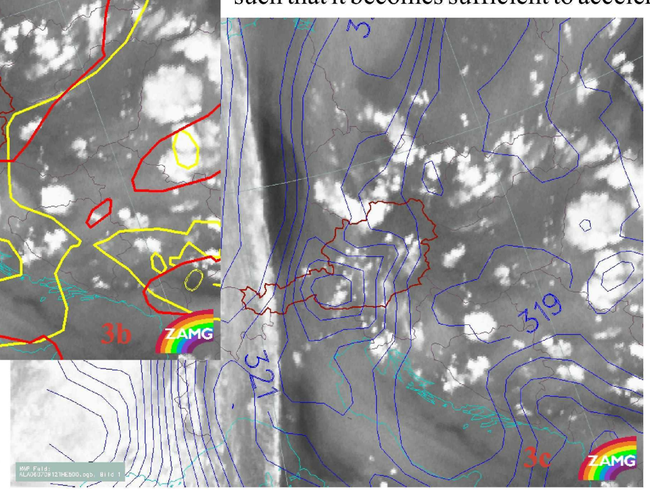

Fig. 3, a - c: MSG Water Vapour channel 6.2µ, 9 July 2006, at 0600 UTC (a) and 1200 UTC (b,c);
3a: ALADIN - LAM model, equivalent potential vorticity, layer 850 - 500 hPa, solid: positive values, dashed: negative values
3b: ALADIN - LAM model, zero line of shear vorticity at 300 hPa (yellow) and 500 hpa (red) depicting wind speed maxima at upper tropospheric levels, indicating distinct vertical wind shear between upper levels and ground
3c: ALADIN - LAM model, Equivalent potential temperature at 500hPa, significant gradient in connection with transitions between moist and dry areas in the WV image (WV boundary)

Significant values of negative EPV_g indicate a possible release of CSI. If a still buoyant and saturated air parcel is reaching a zone of negative EPV_g, CSI might be released leading to an increase of buoyancy. Because of this additional lift the saturated air parcel might reach its level of free convection (LFC). Due to conditional gravitational instability deep convection will result. Vertical acceleration induced by CSI reaches only values from tens of cm/s to a few m/s, whereas gravitational instability provides speeds up to tens of m/s.

During the coexistence of symmetric instabilities and gravitational instabilities, gravitational convection will therefore dominate slantwise convection. But if gravitational convection is weak or moisture supply is inefficient or entrainment causes negative buoyancy or the rising parcel has to surmount a capping inversion, then the release of CSI might modify the convective process such that it becomes sufficient to accelerate the parcel towards its LFC.

Areas within the immediate vicinity of WV boundaries seem to fulfil preconditions necessary for the release of CSI: **1.** Weak gravitational stability in all investigated cases represented by widespread conditional instability and spontaneous convective overturning above ground due to absolute instability. **2.** Dynamical processes lead to local deformation at the WV boundary zone, which promotes EPV_g becoming smaller or negative: EPV_g <0; it is common to all cases, that the onset of DMC takes place within an area of negative values of EPV_g; in **Fig.3a** an area of EPV_g <0 stretches from the Croatian Coast to Poland, which can be related to the turbulent dark feature in the WV image at 0600 UTC prone to succeeding convection activity. Assumingly the release of CSI favourably takes place in those areas at or near saturation: i.e. a saturated buoyant air parcel reaches a zone of distinct negative EPV_g. **3.** The WV boundaries indicate zones with distinct vertical wind shear but little directional shear; **Fig.3b** shows the zero-line of shear vorticity at 500 hPa (red) and 300 hPa (yellow) indicating vertical shear related even to weak WV gradients. **4.** A significant horizontal thermal gradient is induced by the dry and cold intrusion along with the WV dark zone; **Fig.3c** displays the distribution of Θ_e at 500 hPa, a thermal gradient can be related to the WV boundaries.

Assuming WV boundaries fulfil conditions favourable for the release of CSI, the question arises where exactly at an elongated WV boundary the onset of DMC will take place. In addition to areas initially gravitational unstable such regions can be found objectively by the calculation of EPV_g<0 and the increase or decrease of its gradient. It is of interest to analyse the behaviour of conservative field quantities (like EPV_g) within the stream as an indicator for a possible release of CSI. The equivalent-potential temperature undergoes an increase or decrease of its vertical and horizontal gradients. Further the movement of the WV dark stripes or filaments within the flow leads to a change in vertical stability, vertical wind speed, vertical shear conditions and also the horizontal layer distribution of the potential, and equivalent-potential temperature.

In order to assess such changing conditions and thus a change in the behaviour of the EPV_g field an indicating parameter **ν** has been derived (Equation 7), based on the fact that if deformation terms in the geostrophic wind field are dominant, the horizontal gradients of conservative field quantities such as PV, EPV_g and Θ_e are strengthened or weakened.

E7) $$\nu = \left| \frac{\left(E^2 + F^2 - \xi^2\right)}{4} \right|^{\frac{1}{2}}$$

Where **E** is the elongation deformation, **F** is the shear deformation and **ξ** is the relative Vorticity, assuming a divergence free geostrophic flow. The parameter **ν** also provides an indication for turbulence within the stream at a given time and location.

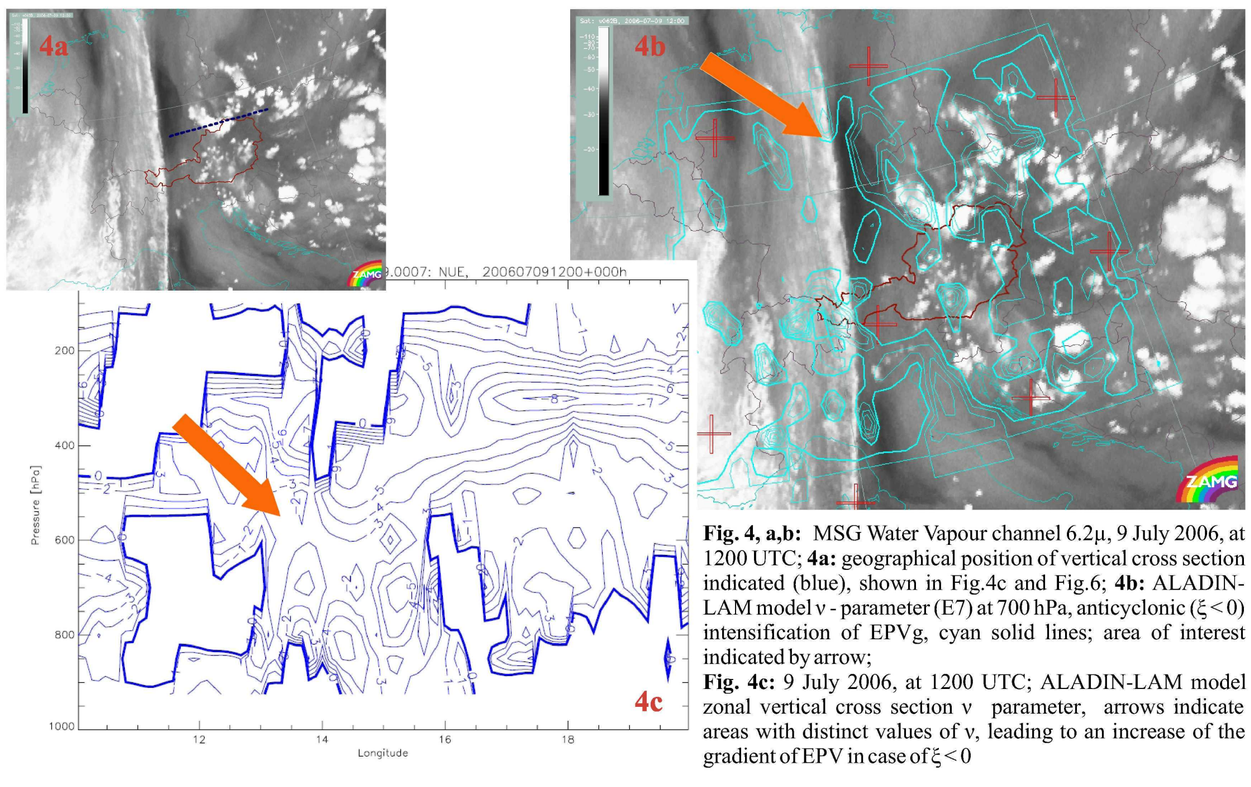

Fig. 4, a,b: MSG Water Vapour channel 6.2µ, 9 July 2006, at 1200 UTC; **4a:** geographical position of vertical cross section indicated (blue), shown in Fig.4c and Fig.6; **4b:** ALADIN-LAM model ν - parameter (E7) at 700 hPa, anticyclonic (ξ < 0) intensification of EPVg, cyan solid lines; area of interest indicated by arrow;
Fig. 4c: 9 July 2006, at 1200 UTC; ALADIN-LAM model zonal vertical cross section ν parameter, arrows indicate areas with distinct values of ν, leading to an increase of the gradient of EPV in case of ξ < 0

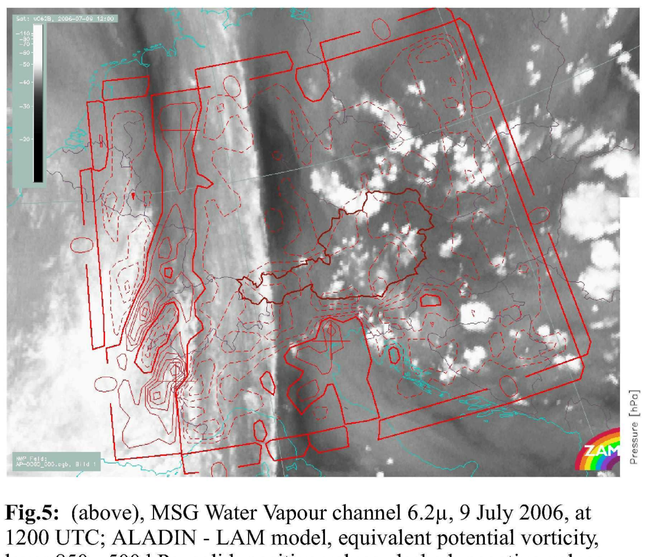

Fig.5: (above), MSG Water Vapour channel 6.2µ, 9 July 2006, at 1200 UTC; ALADIN - LAM model, equivalent potential vorticity, layer 850 - 500 hPa, solid: positive values, dashed: negative values, intensified compared to 6 hours earlier

Fig.6: (below) 9 July 2006, at 1200 UTC; ALADIN-LAM model zonal vertical cross section ν parameter, arrows indicate areas with distinct increase of the gradient of EPV in case of ξ < 0; the geographical position of VCS indicated in Fig.4a

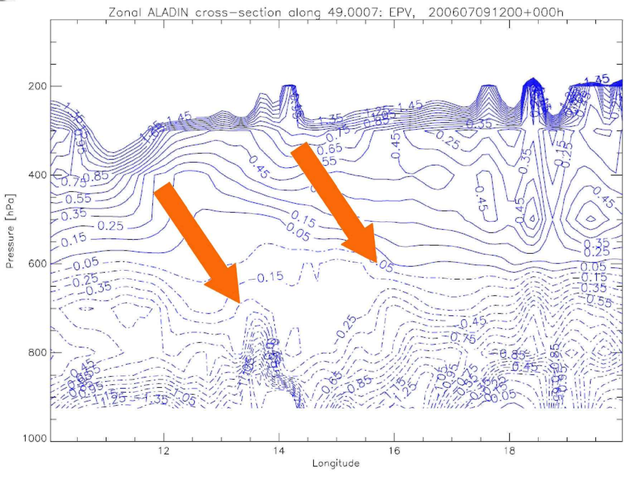

The growth of the magnitude of anticyclonic EPV_g in time proceeds at an exponential rate with **ν** as the governing parameter. But for proper interpretation the deformation terms **E** and **F** or of **ξ** have to be considered individually. The scalar **ν** initially consists of a real and imaginary part and as seen in E7 imaginary solutions are excluded. Furthermore we focus on zones with negative EPV_g, so that mainly anticyclonic areas within high pressure regions are adressed. Therefore regarding equation E7 another limitation is introduced: **ν** is calculated only anticyclonically (ξ < 0, i.e. ξ is set to 0 otherwise) (The case of cyclonic **ν** (ξ > 0) has influence on e.g. frontal zones, post-frontal convection, Comma clouds and enhanced cumuli). The distribution of the **ν** parameter at 700 hPa is shown in **Fig.4b**, the cell complex over northern Austria is well indicated by the parameter. Also the zonal vertical cross section (VCS), indicated in **Fig.4a**, correlates distinct values of ν with the position of the convective cells (**Fig.4c**). The parameter **ν** also indicates areas of intensification of the horizontal gradients of anticyclonic EPV_g in **Fig.5** at 1200 UTC (compared with the state 6 hours before (**Fig.3a**) with weaker gradients, also compare with **Fig.4b**). Since **Fig.5** shows a layer of EPV_g between 850 and 500 hPa, the VCS provides even more distinct values of EPV_g in the lower troposphere (**Fig.6**). Though the involvement of CSI in the onset of DMC at WV boundaries has still to be proven directly, the release of CSI at regions with enhanced anticyclonic EPV_g is highly probable, if a saturated parcel of air reaches such a region. Seen in combination with the gradients in the WV image, a zone favourable to DMC onset can be highlighted at a time before even shallow convection occurs.

References:
HOSKINS, B.J., McIntyre, M.E., Robertson, A.W., 1985: On the Use and Significance of Isentropic Potential Vorticity Maps. *Quart. Journal Roy. Met. Soc., 111*, 877 ff
McCANN, D. W., 1995: Three-dimensional computations of equivalent potential vorticity. *Wea. Forecasting, 10,*798 ff.
SCHULTZ, D. M., and P. N. Schumacher, 1999: The use and misuse of conditional symmetric instability. *Mon.Wea. Rev., 127,* 2709 ff; Corrigendum, *128,* 1573.
Corresponding Author's Address: Central Institute for Meteorology and Geodynamics, Vienna, Austria. Hohe Warte 38, A - 1190 Wien; (1) Operational Forecasting Division, E-mail: t.krennert@zamg.ac.at; (2) Remote Sensing Department, E-mail: a.jann@zamg.ac.at